Effects of self-induced stress on the steady concentration distribution of hydrogen in fcc metallic membranes during hydrogen diffusion

Wu-Shou Zhang,[1,2] Xin-Wei Zhang,[2] and Zhong-Liang Zhang[1]
[1]*Institute of Chemistry & Center for Molecular Science, Chinese Academy of Sciences, P.O. Box 2709, Beijing 100080, China*
[2]*Institute of Applied Physics and Computational Mathematics, P.O. Box 8009, Beijing 100088, China*
(Received 13 October 1999; revised manuscript received 24 March 2000)

Based on the thermodynamics involving the lattice expansion due to hydrogen insertion, the interaction between hydrogen atoms and the blocking effect in hydrogen diffusion, we discuss the profiles of hydrogen concentration and self-induced stress, and their interaction in the steady state during hydrogen diffusion across elastic membranes of fcc metals or alloys. Contrary to the conventional viewpoint, it is found that the self-induced stress suppresses the departure of the concentration distribution from the linearity. The residual stress profile depends on the phase of metal-hydrogen system. However, the diffusion flux is independent of the existence and magnitude of self-stress; this conclusion means that the conventional steady-state method for measurement of the diffusion coefficient can be applied experimentally even while the self-stress effect is significant. Finally, although these results are obtained from the fcc metal-hydrogen system, our conclusions can be extended to the diffusion problem of other interstitials in solid samples.

I. INTRODUCTION

When an external bending is applied to a solid, the induced deformation field will cause interstitials in the sample to move toward expanded areas; this phenomenon is known as the Gorsky effect.[1,2] Moreover, the stress induced by the concentration gradient of interstitials inside a solid without any external bending has a similar effect as well.[3,4] For hydrogen diffusion across metallic membranes, Lewis and coworkers and some other researchers showed that the internal stress results in a flux opposing to that generated by diffusion. This feature has been referred to as ''uphill diffusion.''[5–14] They verified that the self-stress not only leads to a misestimation of diffusion coefficient using the time-lag method,[5–10] but also modifies the steady-state distribution of interstitial in solids (H in metals or alloys in their case).[10–14] This means that one must be cautious about measuring the diffusion coefficient of interstitial in solids either by the transient or steady-state method. However, there still exist some controversies on the problem of the steady-state distribution of interstitial in solids. Li[3] and Baranowski[15] had predicted that the linear profile is the natural result, but some latter theoretical and experimental works supported the concept of the non-linear distribution.[10–14,16,17] In an earlier paper, Zhang *et al.*[18] have proved analytically and numerically that the linear profile is the only solution for interstitial (hydrogen) diffusion across an elastic membrane in the steady state while the metal-hydrogen system is in the phase of dilute solution. Owing to the fact that self-stress experiments are always carried out in the situation of high hydrogen concentration where the interaction between hydrogen atoms and the blocking effect in diffusion must be concerned, so the applicability of this conclusion from the dilute solution condition is in doubt in the practical cases. In this paper, we will further prove that the self-induced stress supresses the departure of the concentration distribution from the linearity, and the diffusion coefficient deduced from the steady-state diffusion flux, plate thickness and concentration step is valid even while the self-stress effect is present. To be specific, we discuss the hydrogen diffusion across a fcc metallic plate because hydrogen in these materials, such as Pd and Pd-based alloys, has been extensively studied in the self-stress experiments.[5–16]

II. MODEL AND RESULTS

According to Refs. 3,4 and 15, the chemical potential of hydrogen interstitial in a metallic lattice (M) under a stress σ can be expressed as

$$\mu_{\mathrm{H}}(x,\sigma)=\mu_{\mathrm{H}}(x,0)-V_{\mathrm{H}}\sigma, \tag{1}$$

where $\mu_{\mathrm{H}}(x,0)$ denotes the chemical potential of hydrogen in the stress-free state ($\sigma=0$) and it plays the role of the standard state with respect to the stress σ; x symbolizes the relative concentration of H in M and is expressed as the atomic ratio of H/M. For fcc metals and alloys above mentioned, H occupies only the octahedral interstitial site and we have $0\leqslant x\leqslant 1$. V_{H} is the partial molar volume of H in M. Referring to Baranowski[19] and Fukai,[20] $V_{\mathrm{H}}=1.69$ cm^3/mol while $x<0.75$ and $V_{\mathrm{H}}=0.18\sim 0.42$ cm^3/mol while $x>0.75$.

The chemical potential of H under the stress-free state in Eq. (1) may be replaced by the expression[20,23]

$$\mu_{\mathrm{H}}(x,0)=\mu_{\mathrm{H}}^{0}+H_{\mathrm{H}}(x)+RT\ln\left(\frac{x}{1-x}\right). \tag{2}$$

The first term in the right-hand side of this equation is the chemical potential of the reference state, the second one is the enthalpy, the third term is the configurational entropy, R is the universal gas constant, T is the absolute temperature in K.

The enthalpy $H_{\mathrm{H}}(x)$ in Eq. (2) changes with x due to the H-H interaction and it is generally a concave function as shown in Fig. 1. It can be expanded in a power series to the first order,

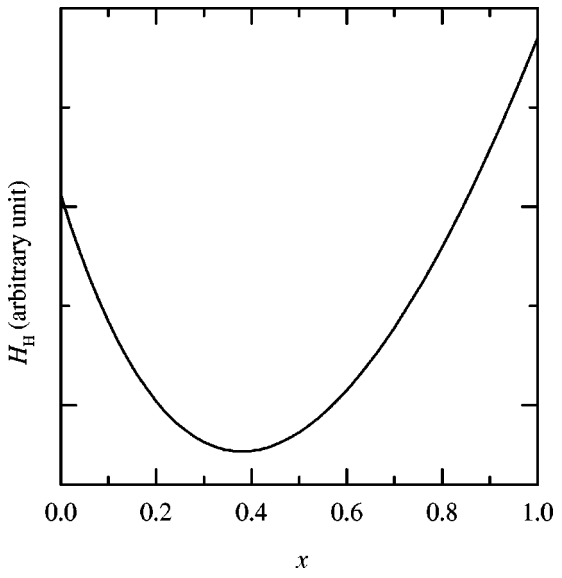

FIG. 1. Schematic picture of hydrogen enthalpy H_H as a function of hydrogen concentration x for H in Pd and Pd-based alloys.

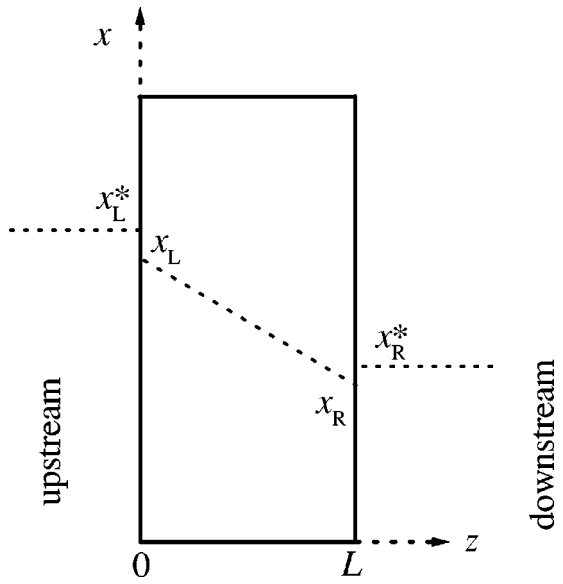

FIG. 2. Schematic picture of hydrogen diffusion across a metallic membrane. Where x is the atomic ratio of H to M; x_L^* and x_R^* are values of x in the stress-free state corresponding to the imposed hydrogen pressure for the gas technique or potential for the electrochemical technique at the upstream and downstream sides, respectively; x_L and x_R are the actual values of x at both sides, respectively.

$$H_H(x)=H_H(x_0)+U_b(x-x_0)+O(x-x_0)^2. \tag{3}$$

The linear approximation indicates that this expression is valid only in a certain range of x near x_0. From the point of view of physics, the change of enthalpy originates from the elastic and electronic interactions between H atoms.[20] The elastic interaction is caused by the dilatation of the metallic octahedral sites arising from the occupying hydrogen atoms and it leads to attractive interactions between H atoms in the lattice. It is found that $U_b=-50\sim-20$ kJ/mol for Pd and Pd-based alloys while $x_0 \ll 1$.[20,21] When x_0 increases to a certain value (its magnitude depends on the sorts of M), the enthalpy decreases to the minimum and it then increases with x_0 up to the saturation absorption ($x_0=1$). The increase of enthalpy with x_0 results from a stepwise in the Fermi energy, which occurs after electrons from the dissolved hydrogen fill the d band of metal and the additional electrons enter the s band.[22] It is found that $U_b=50$ kJ/mol for Pd when $0.6<x_0<0.86$.[23–25]

Similar to the model used in previous papers,[4,15–18] we consider hydrogen diffusion across a thin plate that allows our analysis to be reduced to a one-dimensional problem (see Fig. 2). The self-induced stress is[3,4,15–18]

$$\sigma=-\frac{2V_H Y C_0}{3}\left[x-\frac{1}{L}\int_0^L x\,dz-\frac{12(z-L/2)}{L^3}\times\int_0^L x(z-L/2)\,dz\right], \tag{4}$$

where $Y=E/(1-\nu)$, E is Young's modulus, $E=(1\sim2)\times10^{11}$ Pa, ν is Poisson's ratio, $\nu=0.3\sim0.4$, C_0 is the saturation concentration of H in M corresponding to $x=1$, $C_0=0.1\sim0.15$ mol H/cm^3; L is the plate thickness, z is the coordinate along the diffusion direction, the upstream side is $z=0$ and the downstream side is $z=L$.

As verified experimentally,[20] the mechanism of hydrogen diffusion in fcc metals is the H atom jumping between neighboring octahedral interstitial sites, the blocking factor is $(1-x)$. Thus the hydrogen flux has the form

$$J=-\frac{D_0(1-x)C_0}{RT}\nabla\mu_H(x,\sigma), \tag{5}$$

where $D_0(1-x)$ is the Einstein diffusion coefficient. Introducing Eqs. (1)–(4) into Eq. (5), we obtain the hydrogen flow in the most general form for present purposes:

$$J=-D_0C_0\left[1+\left(\frac{U_b}{RT}+\frac{2V_H^2YC_0}{3RT}\right)x(1-x)\right]\frac{\partial x}{\partial z}+D_0\frac{8V_H^2YC_0^2}{L^3RT}x(1-x)\int_0^L x(z-L/2)\,dz. \tag{6}$$

Applying the mass balance condition to the flux expression gives[26]

$$C_0\frac{\partial x}{\partial t}=-\nabla\cdot J. \tag{7}$$

The boundary condition is[15]

$$\mu_H(x,\sigma)=\mu_H(x^*,0),\quad z=0 \text{ or } L, \tag{8}$$

where x^* is the hydrogen concentration at the outer surfaces corresponding to the imposed hydrogen pressure for the gas phase technique or the potential for the electrochemical technique under the stress-free condition. Equation (8) is similar to the first boundary value condition in some sense as shown in Fig. 2.

For the purpose of analytical and numerical treatment, further analysis is carried out in terms of dimensionless variables and equations. Introduction of the following symbols

$$\xi = z/L, \tag{9}$$

$$\tau = D_0 t/L^2, \tag{10}$$

$$j = \frac{LJ}{D_0 C_0}, \tag{11}$$

$$u_b = \frac{U_b}{RT}, \tag{12}$$

$$\sigma_0 = \frac{2}{3} V_H Y C_0, \tag{13}$$

and

$$u_\sigma = \frac{V_H \sigma_0}{RT}, \tag{14}$$

where u_b, σ_0, and u_σ are material constant. u_b is the H-H interaction factor; σ_0 is the maximum self-induced stress; u_σ is the self-stress factor. Using the values mentioned above, we have $u_b = -20$–20, $\sigma_0 = 1.7$–56 GPa, and $u_\sigma = 0.1$–40 at room temperature. Besides the variables in Eqs. (9)–(14), we introduce another quantity, $A(\tau)$, defined as

$$A = -12 \int_0^1 x(\xi - 1/2) d\xi. \tag{15}$$

Thus Eqs. (4) and (6)–(8) can be simplified to

$$\frac{\sigma}{\sigma_0} = -\left[x - \int_0^1 x d\xi + A(\xi - 1/2) \right], \tag{16}$$

$$j = -[1 + (u_b + u_\sigma) x(1-x)] \frac{\partial x}{\partial \xi} - A u_\sigma x(1-x), \tag{17}$$

$$\frac{\partial x}{\partial \tau} = -\frac{\partial j}{\partial \xi}, \tag{18}$$

and

$$\left[\frac{x}{1-x} \exp(u_b x) \right] \Big/ \left[\frac{x^*}{1-x^*} \exp(u_b x^*) \right] = \exp\left\{ -u_\sigma \left[x - \int_0^1 x d\xi + A(\xi - 1/2) \right] \right\},$$

$$\xi = 0 \text{ or } 1, \tag{19}$$

respectively.

We attempt to analytically solve these equations in the steady-state diffusion. Because A and j are all time independent in the case, Eq. (17) is reduced to an ordinary differential equation and x is uniquely determined by ξ. Integrating Eq. (17) with respect to ξ from ξ to 1 by separation of variables leads to

$$(1-\xi) = \frac{u_b + u_\sigma}{A u_\sigma}(x - x_R) - \frac{1}{w}\left[1 - \frac{(u_b + u_\sigma) j}{A u_\sigma} \right] \times \ln\left[\frac{A u_\sigma (1-2x) + w}{A u_\sigma (1-2x) - w} \frac{A u_\sigma (1-2x_R) - w}{A u_\sigma (1-2x_R) + w} \right] \tag{20}$$

with

$$w^2 = (A u_\sigma)^2 + 4 A u_\sigma j. \tag{21}$$

x as a function of ξ can be iteratively solved through combining Eqs. (15) and (19)–(21). Assume a set of values, j, x_R, and A, new values of x_R and A can be iteratively extracted by combining Eqs. (15), (20), and (21). Adjust j and repeat the above procedure up to the resulted x_L^* being equal to the known value. Numerical results shown in the table and figures of this paper are calculated using this method. For the sake of contrast, we do not directly show x but illustrate its departure from the ideal linear distribution

$$d_x = x - [x_L^* - (x_L^* - x_R^*)\xi] \tag{22}$$

in the figures.

Another way of obtaining x is to numerically solve the partial integro-differential Eqs. (15)–(19), the desired solution is acquired when τ is large enough ($\tau \gg 1$). Of course, results achieved by these two methods are consistent with each other.

For understanding this phenomenon more clearly, we give the series solution in the below. First of all, rigorous results can be obtained for two special situations. One is for $u_\sigma \to 0$, solution of Eq. (17) is

$$j(1-\xi) = (x - x_R^*) + \frac{u_b}{2}(x^2 - x_R^{*2}) - \frac{u_b}{3}(x^3 - x_R^{*3}). \tag{23}$$

The corresponding numerical results are shown by dotted curves in Figs. 3–6. We find they are all the most bent curves and the magnitude of nonlinear part is much less than that of the linear one while x is large.

Another special case is for $u_b \to 0$, there is

$$j(1-\xi) = (x - x_R^*). \tag{24}$$

This is the linear solution as has been discussed in the earlier studies[3,15,18] although the blocking effect in diffusion and the configuration entropy in chemical potential of hydrogen are involved here. An example of this solution, the horizontal dotted line, is shown in Fig. 3(a). For a more general situation, a power series expansion for x about the point $\xi = 1/2$ to the third order gives

$$x = x_m + a_1(\xi - 1/2) + a_2(\xi - 1/2)^2 + a_3(\xi - 1/2)^3 + O(\xi - 1/2)^4, \tag{25}$$

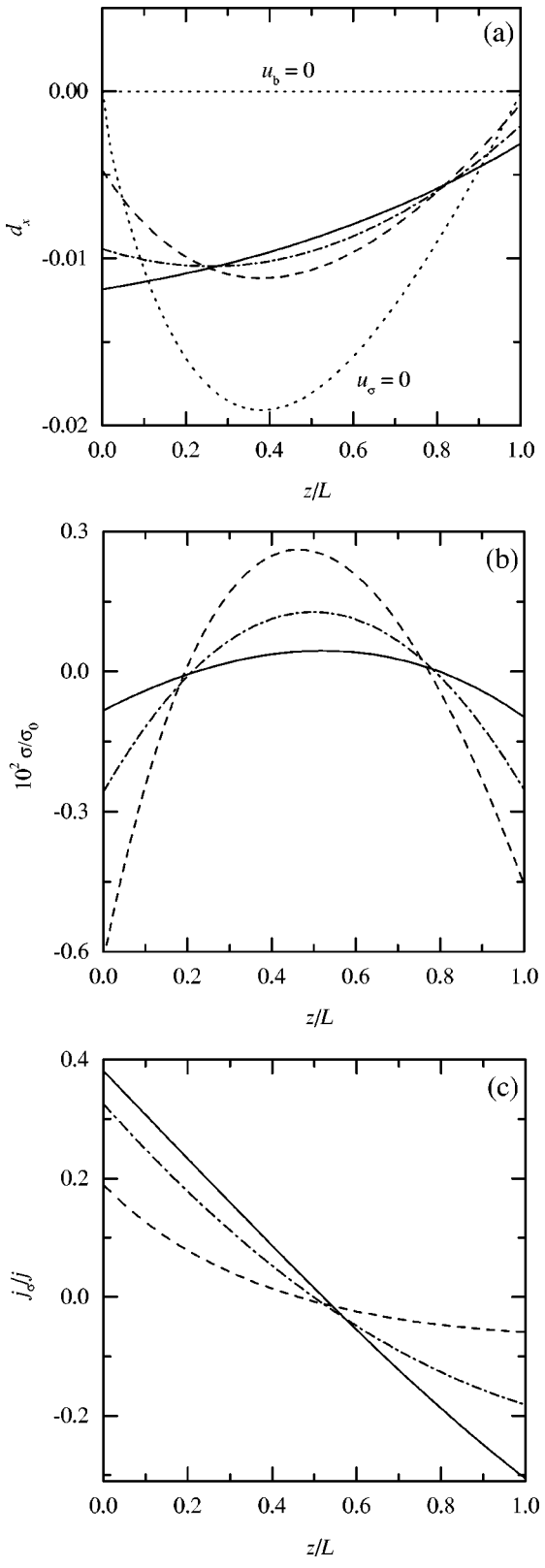

FIG. 3. Numerical results of profile of hydrogen concentration, self-stress and stress-induced flux during hydrogen steady diffusion across a plate. (a) Departure of hydrogen concentration distribution from the ideal linearity, $d_x = x - [x_L^* - (x_L^* - x_R^*)z/L]$, (b) profiles of the relative residual self-stress σ/σ_0, and (c) profiles of the relative stress-induced flux j_σ/j. The dashed, dash-dot and solid lines are for u_σ = 1,5, and 20, respectively. The other parameters: $x_L^* = 0.2$, $x_R^* = 0.1$ and $u_b = -5$.

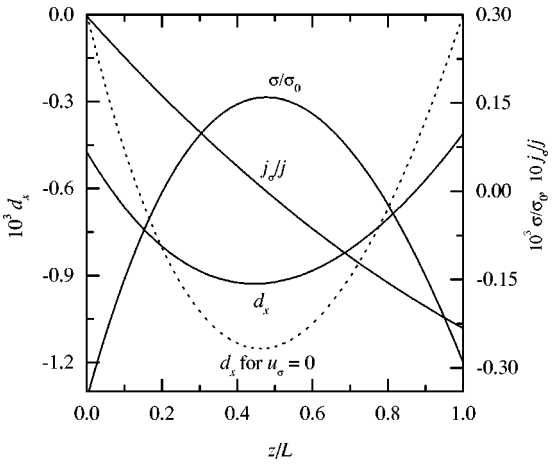

FIG. 4. An example similar to Fig. 3 but with different parameters: $x_L^* = 0.7$, $x_R^* = 0.6$, $u_b = 10$, and $u_\sigma = 20$.

where x_m is the value of x in the central plane $\xi = 1/2$. As a crude approximation, x_m can be replaced by the average value of x_L and x_R. Substituting this equation into Eq. (15) gives

$$A = -a_1 \tag{26}$$

in the second-order approximation. Introducing Eqs. (25) and (26) into Eq. (17), we obtain the expansion coefficients

$$a_1 \approx -\frac{j}{1 + u_b x_m (1 - x_m)}, \tag{27}$$

$$a_2 = -\frac{1}{2}\frac{u_b(1 - 2x_m)}{1 + (u_b + u_\sigma)x_m(1 - x_m)} a_1^2, \tag{28}$$

and

$$a_3 = -\frac{1}{3}\frac{a_1^3 u_b - a_1 a_2 (3u_b + 2u_\sigma)(1 - 2x_m)}{1 + (u_b + u_\sigma)x_m(1 - x_m)}. \tag{29}$$

From Eq. (27), we find that a_1 is out of relation to u_σ, this means that the linear part of the concentration distribution is independent of the self-stress. By Eqs. (28) and (29), we find that a_2 and $a_3 \to 0$ when $u_b \to 0$ or $u_\sigma \to \infty$. The former con-

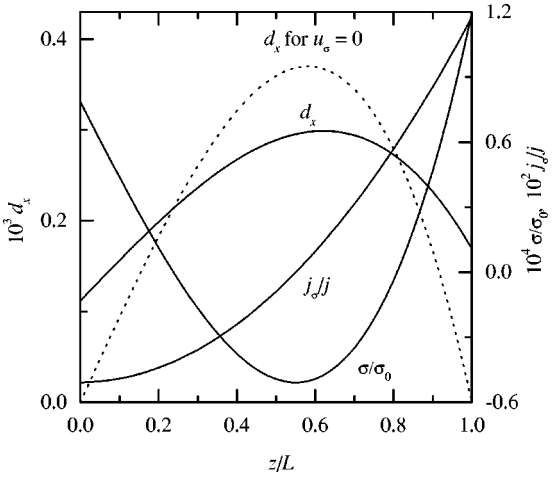

FIG. 5. An example similar to Fig. 3 but with different parameters: $x_L^* = 0.5$, $x_R^* = 0.4$, $u_b = 10$, and $u_\sigma = 20$.

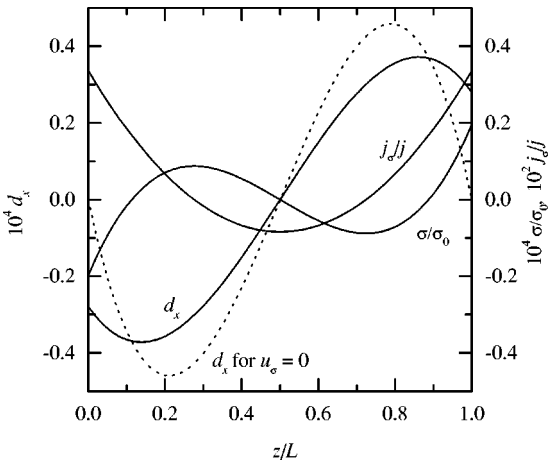

FIG. 6. An example similar to Fig. 3 but with middle values of hydrogen concentration. The parameters: $x_L^*=0.55$, $x_R^*=0.45$, $u_b=10$, and $u_\sigma=20$.

dition makes Eq. (25) equivalent to Eq. (24) and the latter case means that the self-stress suppresses the departure of concentration distribution from linearity as illustrated in Figs. 3–6. Of course, Eq. (25) is reduced to the series solution of Eq. (23) when $u_\sigma \to 0$.

Substituting Eq. (25) into Eqs. (15) and (16), we obtain the residual self-stress in the steady-state,

$$\frac{\sigma}{\sigma_0}=a_2\left[\frac{1}{12}-\left(\xi-\frac{1}{2}\right)^2\right]+a_3\left(\xi-\frac{1}{2}\right)\left[\frac{3}{20}-\left(\xi-\frac{1}{2}\right)^2\right]. \tag{30}$$

Because the linear concentration profile gives the zero stress, the residual self-stress arises from the nonlinear part of the concentration distribution. In the second-order approximation, only the term with a_2 is left; the self-stress is symmetrical about the central plane of plate and $\sigma=0$ at $\xi=0.21$ and 0.79 which explain why several stress curves in Fig. 3(b) seem to intersect at these two points on the zero stress axis. Figure 3(b) reveals that the second-order approximation is appropriate while the self-stress factor u_σ is large enough.

The stress-induced flux is

$$j_\sigma=a_2u_\sigma x(1-x)(1-2\xi)+a_3u_\sigma x(1-x)\left[\frac{3}{20}-3\left(\xi-\frac{1}{2}\right)^2\right]. \tag{31}$$

As a second-order approximation, this expression and results shown in Figs. 3–5 indicate that the stress-induced flux increases with increasing u_σ, and j_σ has opposite contributions to the overall flux in the two different half regions ($0<\xi<1/2$ and $1/2<\xi<1$).

Figures 3–6 show the numerical results of d_x, σ/σ_0 and j_σ/j as functions of ξ with different parameters. Examples shown in Fig. 3 are for the dilute solution of H in M (α phase, $u_b<0$). The situation of hydride phase (β phase, $u_b>0$) is shown in Fig. 4; we find that the relative quantities of the self-stress and stress-induced flux are much less than those in the α phase. This is because that a_2 is very small when $u_b>0$ as indicated by Eq. (28). From the point of view of thermodynamics, the chemical potential increases sharply with x while $x>1/2$ as discussed above and shown in Fig. 1. Therefore the relative contribution of self-stress to the total chemical potential decreases with increasing x, as well as the self-stress effect.

Although Figs. 3 and 4 show two different situations, they have the same feature, i.e., $d_x<0$ or x is a concave function of ξ. The solid samples bear the compressive stress near surfaces and the tensile stress in the central region as before illustrated in the hydrogen absorption process.[3,16] However, we find that the contrary situation can occur when $a_2<0$ in Eq. (30), which corresponds to $u_b>0$ and $x_m<1/2$, or $u_b<0$ and $x_m>1/2$ as indicated by Eq. (28). Figure 5 shows an example of this situation, it is found that the H concentration distribution is slightly protrusive and x is great than the ideal linear case ($d_x>0$). The self-stress and stress-induced flux are in contrast with those of Figs. 3 and 4. In experiments, this situation can be realized by raising temperature or using some alloys, so the miscibility gap of different phases disappears and only one phase exists. Formally, if $x_m>1/2$ and $u_b<0$, there will be the similar result but this situation is rare because $u_b>0$ while x is large.

Another interesting phenomenon occurs when $x_m=1/2$ as illustrated in Fig. 6. In the case, the stress effect must be described by the third-order approximation due to $a_2=0$. The nonlinear part of the concentration distribution and the stress profile have third-order characteristics, and the stress-induced flux has a quadric form as indicated by Eqs. (25), (30), and (31), respectively. Different features between Fig. 6 and Figs. 3–5 make us obtain the condition

$$\left|\frac{a_2}{a_3}\right| \gg 1 \tag{32}$$

under which the second-order approximation is valid; otherwise, the third-order approximation must be considered. Introducing Eqs. (28) and (29) into this equation and neglecting the higher-order terms, we get the condition being equivalent to Eq. (32),

$$|x_m-1/2| \gg |a_1|/3. \tag{33}$$

This criteria is based on the series expansion about the middle point $\xi=1/2$. Actually, x can be expanded at any point in the overall range of $0\leqslant\xi\leqslant1$, so we find that $a_2=0$ if $x=1/2$ at the point expanded from Eq. (28), so we obtain the necessary condition for consideration of the third-order approximation

$$x_L^*>1/2>x_R^*. \tag{34}$$

Otherwise, the second-order approximation is enough to describe the self-stress effects.

III. DISCUSSION AND CONCLUSION

By Figs. 3–6, we find that the self-stresses flatten the nonlinear distribution and it presents a striking contrast to other researchers' prediction;[10–14,16,17] this phenomenon can be understood through the stress distribution. For the concave profile of x vs ξ, the stress distribution is protruding. Because a stress-induced flux j_σ is proportional to the gradient of stress, so j_σ is positive and negative in the left and right regions, respectively. This means that the self-stresses make the pit of concentration departure from the linearity to

TABLE I. Numerical data of example shown in figures of this paper.

n	x_L^*	x_R^*	u_b	u_σ	x_L	x_R	A	j
3	0.2	0.1	0	−	0.2	0.1	0.1	0.1
			−5	0	0.2	0.1	0.1	0.0366667
				1	0.195278	0.0992552	0.0944337	0.0366566
				5	0.190580	0.0979614	0.0925817	0.0366443
				20	0.188163	0.0968829	0.0914314	0.0366367
4	0.7	0.6	10	0	0.5	0.4	0.1	0.326667
				20	0.699525	0.599590	0.0998750	0.326667
5	0.5	0.4	10	0	0.5	0.4	0.1	0.346667
				20	0.500112	0.400169	0.0999017	0.346667
6	0.55	0.45	10	0	0.55	0.45	0.1	0.349167
				20	0.549972	0.40028	0.0999047	0.349167

[a] n is the figure number in this paper.

be filled in. Similarly, the same mechanism can explain that the stresses make the pile of concentration departure from the linearity to be cut out as shown in Figs. 5 and 6. In previous works, it was considered theoretically[16,17] and verified experimentally[10–14] that the self-stresses make the hydrogen distribution has a concave shape or S shape along the diffusion direction in plates. Our results demonstrate the contrary situation, i.e., the concave, protruding and S shape profiles of hydrogen content under the stress-free condition will be straightened by the self-stresses. It indicates that the corresponding experimental results associated with the ''nonlinear distribution'' need further interpretation using other mechanisms. On the other hand, our results show that the linear profile of hydrogen concentration is a good approximation for the steady-state diffusion in an elastic membrane. Although these results are obtained from the system of hydrogen in fcc metals or alloys, this mechanism and conclusion can be extended to all sorts of interstitials in solids.

Another striking feature of our results is that the fluxes almost maintains constant values either for self-stress is absent or present, weak or strong as shown in Table I. The reason is that the diffusion flux is determined by the gradient of the chemical potential as indicated by Eq. (5), and it should be constant for fixed imposed boundary conditions. Despite the self-stress modifies the local concentration of interstitial, the chemical potential and its gradient, which corresponds to the interstitial flux, do not change with self-stress in the steady state. For practical cases, this means that the average diffusion coefficient can be measured by the relation $D=LJ/\Delta C$ (ΔC is the concentration difference across the diffusion membrane) and it is independent of whether the self-induced stress is concerned or not. Of course, the boundary condition of Eq. (8) must be satisfied; in other words, the interface process must be fast enough to reach the pseudoequilibrium.

A basis of our model is that the sample consists of dislocation-free crystals and all stresses created are not relaxed at grain boundaries or by plastic flow. The validity of this assumption in experiments depends on the sort of material, processing of material preparation and specific condition. Nevertheless, some conclusion can be reached from our results as discussed above. We find that the maximum self-stress in our model is in the order of 10 MPa which is less than the yield stress of most materials, therefore the stress may be maintained for a long time. Another fact is that the magnitude of self-stress decreases with the increasing of hydrogen concentration as shown in Figs. 3–6, this means the self-stress effect is not prominent at the high hydrogen concentration as discussed above.

In summary, we have established a model describing hydrogen diffusion across an elastic fcc metallic plate. This model includes the self-stress effect of hydrogen insertion, H-H interaction and blocking effect in diffusion. The results indicate that the self-stress flattens the nonlinear distribution of hydrogen concentration in the plate and it is contrary to the conventional viewpoint. On the other hand, the diffusion flux maintains constant even while the self-stress effect is present.

ACKNOWLEDGMENTS

This work was supported by the Natural Science Foundation of China under Grant No. 19455001, the Pan-Deng Project of the Department of Science and Technology of China under Grant No. 95-yu-41, the President's Foundation of the Chinese Academy of Sciences, and the Foundation of the China Academy of Engineering Physics.

[1] J. Völkl, Ber. Bunsenges. Phys. Chem. **76**, 797 (1972); J. Völkl and G. Alefeld, Z. Phys. Chem., Neue Folge **114**, 129 (1979).
[2] H. Wipf, J. Less-Common Met. **49**, 291 (1976).
[3] J.C.M. Li, Metall. Trans. A **8**, 1353 (1978).
[4] F.C. Larché and J.W. Cahn, Acta Metall. **21**, 1051 (1973); **30**, 1835 (1982); **33**, 331 (1985); Acta Metall. Mater. **40**, 947 (1992); Solid State Phenom. **3-4**, 205 (1988).
[5] F.A. Lewis, J.P. Magennis, S.G. McKee, and P.J.M. Seebuwufu, Nature (London) **306**, 673 (1983).
[6] F.A. Lewis, X.Q. Tong, R.V. Bucur, and K. Kandasamy, Defect

Diffus. Forum **148-149**, 161 (1997).
[7] X.Q. Tong, K. Kandasamy, and F.A. Lewis, Scr. Metall. Mater. **24**, 1923 (1990); X.Q. Tong, Y. Sakamoto, F.A. Lewis, R.V. Bucur, and K. Kandasamy, Int. J. Hydrogen Energy **22**, 141 (1997).
[8] Y. Sakamoto, H. Tanaka, F.A. Lewis, X.Q. Tong, and K. Kandasamy, Int. J. Hydrogen Energy **21**, 1025 (1996).
[9] Dudek and B. Baranowski, Pol. J. Chem. **69**, 1196 (1995); Z. Phys. Chem., Neue Folge **206**, 21 (1998).
[10] K. Kandasamy, X.Q. Tong, and F.A. Lewis, J. Phys.: Condens. Matter **4**, L439 (1992); K. Kandasamy and F.A. Lewis, Int. J. Hydrogen Energy **24**, 763 (1999).
[11] Y. Sakamoto, X.Q. Tong, and F.A. Lewis, Scr. Metall. Mater. **25**, 1629 (1991).
[12] K. Kandasamy, F.A. Lewis, J.P. Magennis, S.G. McKee, and X.Q. Tong, Z. Phys. Chem., Neue Folge **171**, 213 (1991).
[13] F.A. Lewis and X.Q. Tong, J. Alloys Compd. **179**, 13 (1992); F.A. Lewis, X.Q. Tong, and K. Kandasamy, Int. J. Hydrogen Energy **18**, 481 (1993); F.A. Lewis, X.Q. Tong, K. Kandasamy, R.V. Bucur, and Y. Sakamoto, Thermochim. Acta **218**, 57 (1993).
[14] X.Q. Tong and F.A. Lewis, Int. J. Hydrogen Energy **20**, 641 (1995).
[15] B. Baranowski, J. Less-Common Met. **154**, 329 (1989); in *Flow, Diffusion and Processes*, edited by S. Sieniutycz and P. Salaman, Advances in Thermodynamics Vol. 6 (Taylor and Francis, New York, 1992), p. 168.
[16] K. Kandasamy, Scr. Metall. **22**, 479 (1988); Int. J. Hydrogen Energy **20**, 455 (1995).
[17] A.M. Simon and Z.J. Grzywna, Acta Metall. Mater. **40**, 3465 (1992); A.M. Simon, Int. J. Hydrogen Energy **22**, 27 (1997).
[18] W.S. Zhang, X.W. Zhang, and Z.L. Zhang, J. Alloys Compd. **302**, 258 (2000).
[19] B. Baranowski, S. Majchrzak, and T.B. Flanagan, J. Phys. F: Met. Phys. **1**, 258 (1971).
[20] Y. Fukai, *The Metal-Hydrogen System, Basic Bulk Properties* (Springer-Verlag, Berlin, 1993), Chaps. 3 and 5.
[21] Y. Sakamoto, F.L. Chen, and T.B. Flanagan, Ber. Bunsenges. Phys. Chem. **99**, 807 (1995).
[22] D.A. Papaconstantopoulos, B.M. Klein, E.N. Economou, and L.L. Boyer, Phys. Rev. B **17**, 141 (1978).
[23] E. Wicke and G. Nernst, Ber. Bunsenges. Phys. Chem. **68**, 224 (1964); E. Wicke and H. Brodowsky, in *Hydrogen in Metals*, edited by G. Alefled and J. Völkl, Topics in Applied Physics Vol. 29 (Springer-Verlag, Berlin, 1978), p. 73; E. Wicke and J. Blaurock, Ber. Bunsenges. Phys. Chem. **85**, 1091 (1981).
[24] T. Kuji, W.A. Oates, B.S. Bowerman, and T.B. Flanagan, J. Phys. F: Met. Phys. **13**, 1785 (1983).
[25] Y. Sakamoto, M. Imoto, K. Takai, T. Yanaru, and K. Ohshima, J. Phys.: Condens. Matter **8**, 3229 (1996).
[26] J. Crank, *The Mathematics of Diffusion* (Clarendon, Oxford, 1975), p. 3.